Supporting Information

Ligand-induced Changes in the Electrocatalytic Activity of Atomically Precise Au_{25} Nanoclusters

Lipan Luo,[a][+] Xia Zhou,[b][+] Yuping Chen,[a] Fang Sun,[a] Likai Wang*[b] and Qing Tang*[a]

[a] School of Chemistry and Chemical Engineering, Chongqing Key Laboratory of Chemical Theory and Mechanism, Chongqing University, Chongqing 401331, China.

[b] School of Chemistry and Chemical Engineering, Shandong University of Technology, Zibo, Shandong, 255049, China

*To whom correspondence should be addressed. E-mail: lkwangchem@sdut.edu.cn; qingtang@cqu.edu.cn

[+] These two authors contributed equally to this work.

Computation details

Constant-potential method. To calculate the free energies of species involved in electrochemical reactions, we employed a constant-potential method (CPM) while accounting for solvent effects using the implicit solvation model provided by VASPsol. To illustrate the Δ*G* calculation using CPM, we use the Volmer reaction from HER as an example, where a proton from the solution adsorbs onto the catalyst surface, coupled with electron transfer from the electrode.

In the charge-neutral method (CNM), the Gibbs free energy change (Δ*G*) for the reaction $H^+(sol) + e^- \rightarrow H^*$ is calculated as:

$$\Delta G_{cnm} = G(*H) - G(*) - G(H^+(sol)) - \mu_e \quad (1)$$

where *G*(H*) and *G*(*) are the free energies of the catalyst with and without hydrogen adsorption, respectively, *G*(H^+(sol)) is the free energy of the proton in solution at given pH; and μe is the electron energy, which is defined by the absolute electrode potential.

To make this calculation more computationally feasible, μ_e is referenced to the electron energy in the standard hydrogen electrode (SHE), denoted as μ_{SHE}, and the Nernst equation is applied. This reformulates the Δ*G* expression as:

$$\Delta G_{cnm} = G(*H) - G(*) - G(H_2)/2 + |e|U \quad (2)$$

When employing the constant-potential method, which accounts for the varying charge states of the catalyst during the reaction, the Δ*G* calculation is modified as:

$$\Delta G_{cpm} = G_{sol}(*H^{Q2}) - G_{sol}(*^{Q1}) - G(H_2)/2 + |e|U + (Q2 - Q1)\mu_e \quad (3)$$

where Q1 and Q2 represent the net charges on the catalyst before and after hydrogen adsorption, determined by the condition

$$E_F(*^{Q1}) = E_F(*H^{Q2}) = \mu_e \quad (4)$$

where E_F is the Fermi energy. The electron energy μ_e is calculated as:

$$\mu_e = \mu_{SHE} - |e| \cdot U_{SHE} \quad (5)$$

where U_{SHE} is the applied potential versus SHE, benchmarked to be −4.6 eV in VASPsol.[1]

The relationship between U_{RHE} and U_{SHE} is given by:

$$U_{RHE} = (\Phi - \Phi_{SHE})/e + 0.0592 \times pH \quad (6)$$

where Φ is the work function, determined by the energy difference between the vacuum level and the Fermi level. This relationship enables the calculation of the potential U by adding extra electrons. This approach allows us to model the potential-dependent free energy as a quadratic function $G(U)$, facilitating the analysis of reaction energy changes with varying potential.

To represent the constant-potential conditions, extra electrons are systematically added or removed to control the surface charge state. In evaluating the reaction barriers, the potential is calculated as the average of the potentials at the initial (U_{IS}) and final states (U_{FS}):

$$U_r = (U_{IS} + U_{FS}) / 2$$

This ensures the calculated free energy at constant potential accurately reflects the reaction environment, as outlined in earlier studies.[2, 3]

Slow-growth approach. In the thermodynamic integration (TI) method, the reaction free energy and kinetic barrier are obtained by applying a holonomic constraint on the reaction coordinate (ζ) during MD simulations and integrating over the average unbiased force associated with the reaction coordinate,[4, 5] The free energy difference between two reaction coordinates (ζ_a and ζ_b) is given by:

$$\Delta A(\zeta_a, \zeta_b) = -\int_{\zeta_a}^{\zeta_b} F(\zeta) d\zeta \quad (7)$$

Where $\Delta A(\zeta_a , \zeta_b)$ is the free energy difference between two reaction coordinates ζa and ζb and $F(\zeta)$ is the averaged constrained force along the reaction coordinate.

For the formation of H_2 in the second step of the HER ($*H + H_3O + e^- \rightarrow * + H_2 + H_2O$), the CV is defined as:

$$CV = \zeta(r) = |r_{Au(surface)} - r_{HA}| + |r_{Au(staple)} - r_{HA}| - |r_{HA} - r_{HB}| \quad (8)$$

where r_{HA} refers to the coordinate of the H atom adsorbed at the Au bridge site, and r_{HB} refers to the coordinate of the H atom on the hydronium ion (H_3O^+).

For the formation of *CO under alkaline conditions ($*COOH \rightarrow *CO + OH^-$), the

CV is defined as:

$$CV = \zeta(r) = |r_C - r_O| \quad (9)$$

where r_C refers to the coordinate of the C atom on the *COOH, and r_O refers to the coordinate of the O on the -OH group of *COOH.

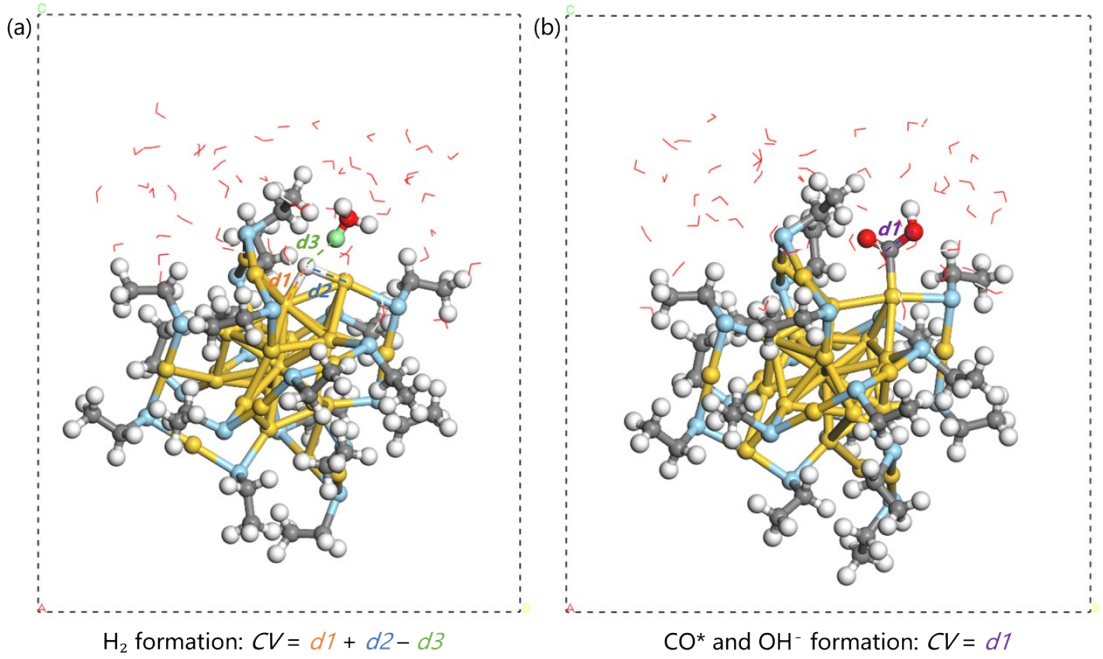

Fig. S1 Illustration of individual and collective variable used as reaction coordinates in the "slow-growth" approach. The specific reactions depicted are: (a) H_2 formation and (b) formation of CO* and OH^-.

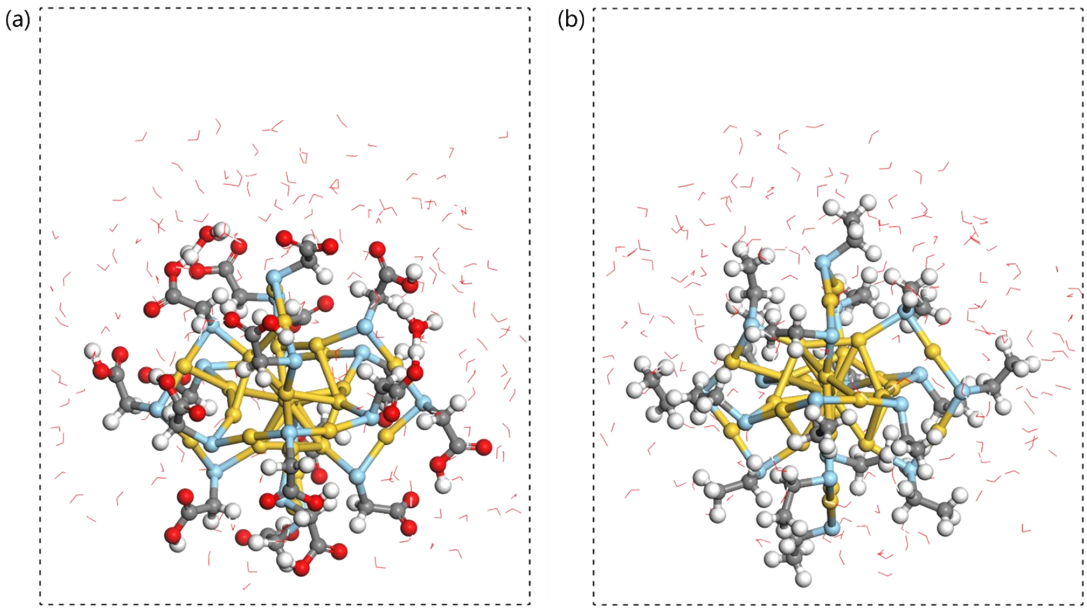

Fig. S2 Optimized structures of (a) $[Au_{25}(SCH_2COOH)_{18}]^-$ and (b) $[Au_{25}(SCH_2CH_3)_{18}]^-$, with the simulation box filled with water to simulate acidic conditions (191 H_2O molecules and one H_3O^+ ion).

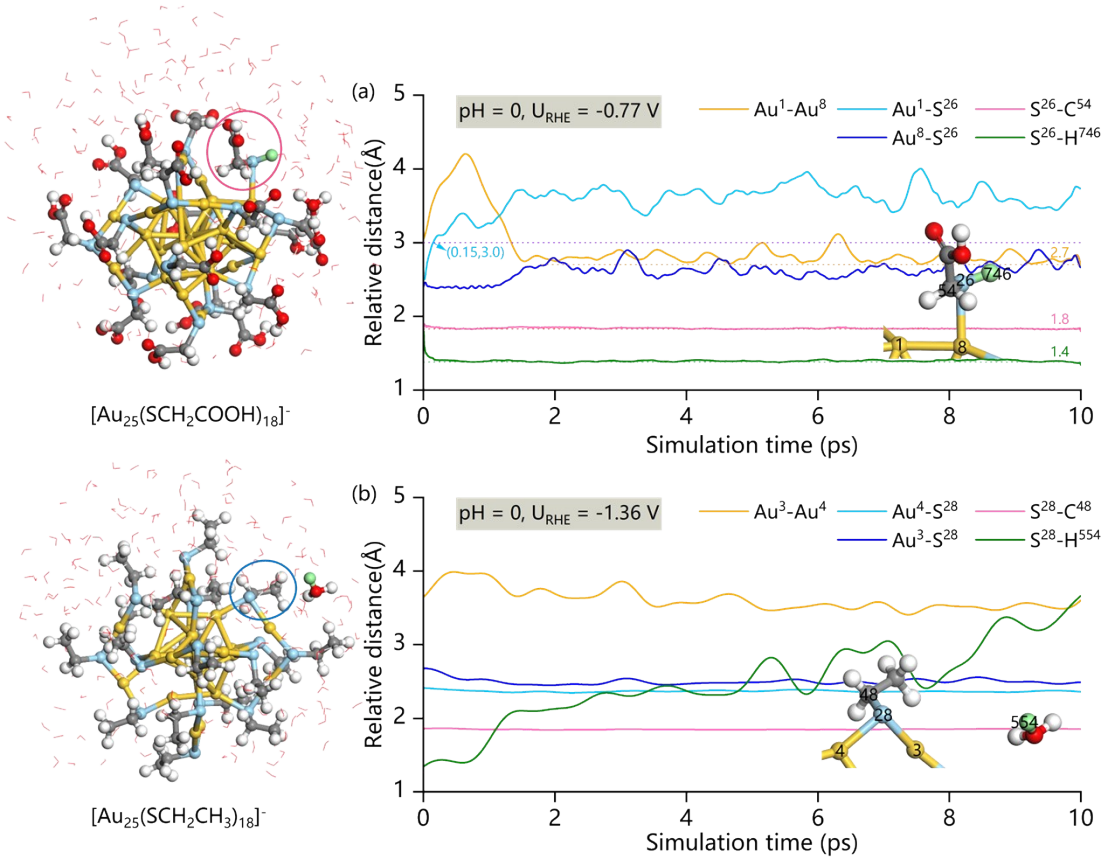

Fig. S3 Relative distances between representative atoms during the equilibrated AIMD simulations at 300 K with the introduction of one extra electron in an acidic environment (pH = 0) for (a) $[Au_{25}(SCH_2COOH)_{18}]^-$ and (b) $[Au_{25}(SCH_2CH_3)_{18}]^-$.

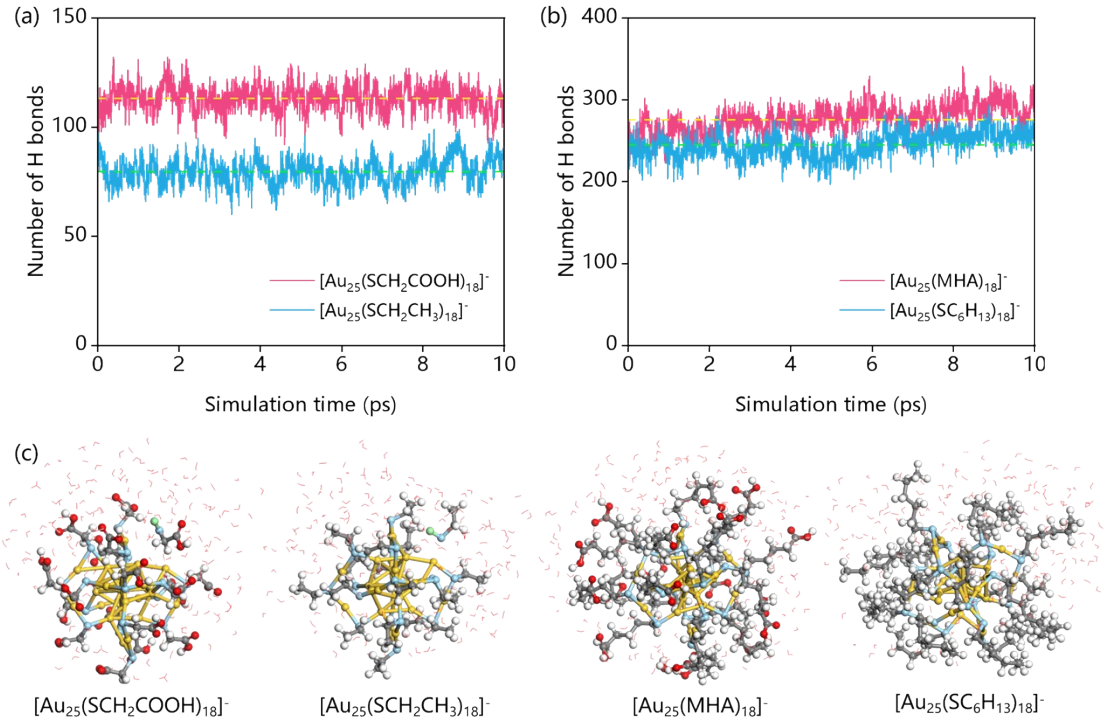

Fig. S4 Comparison in the number of hydrogen bonds in (a) $[Au_{25}(SCH_2COOH)_{18}]^-$ and $[Au_{25}(SCH_2CH_3)_{18}]^-$, as well as (b) $[Au_{25}(MHA)_{18}]^-$ and $[Au_{25}(SC_6H_{13})_{18}]^-$ during equilibrated AIMD simulations at 300 K in an acidic environment (pH = 0) after the introduction of two extra electrons. (c) The snapshots of the four Au_{25}/water structures after 10ps AIMD simulations.

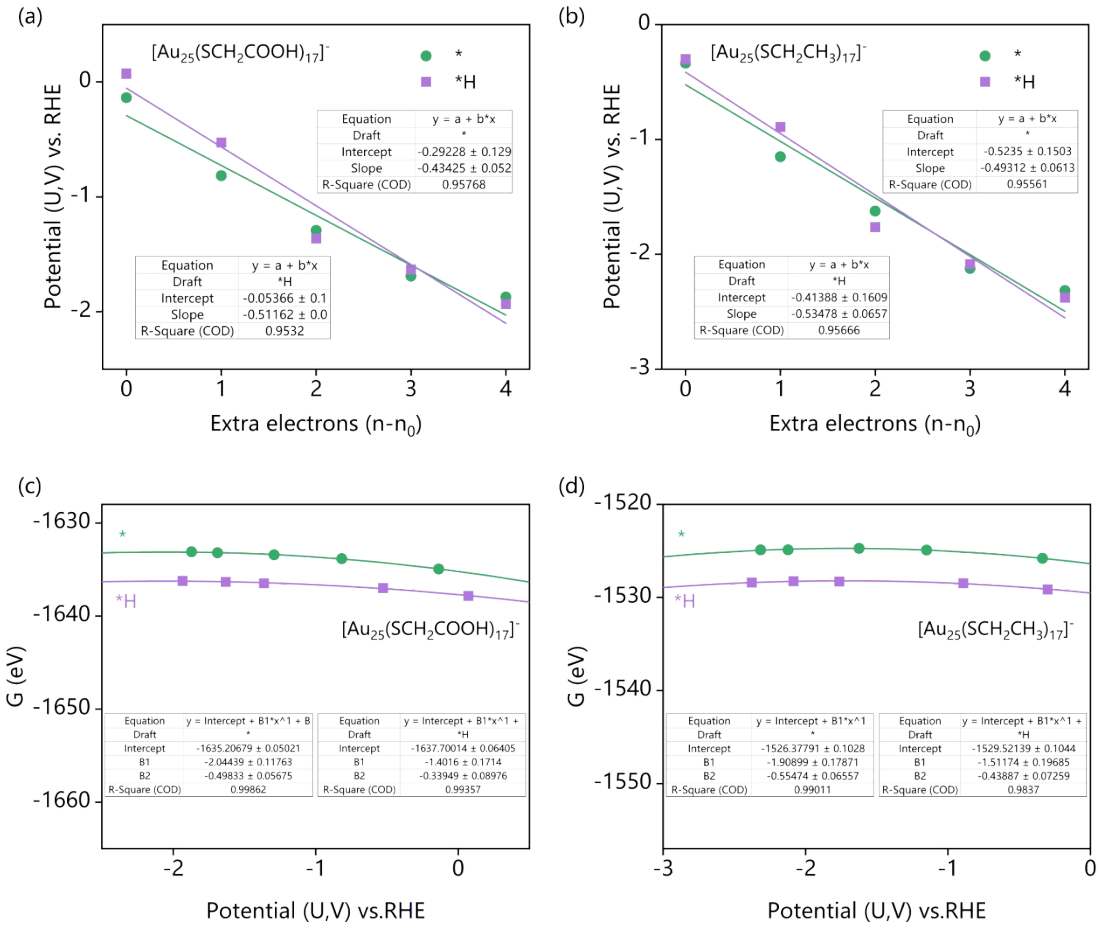

Fig. S5 The relationship between the number of extra electrons ($n–n_0$) and the corresponding electrode potentials for (a) $[Au_{25}(SCH_2COOH)_{17}]^-$ and (b) $[Au_{25}(SCH_2CH_3)_{17}]^-$ in the H_2 formation step of the HER process. Variation in Gibbs free energy as a function of electrode potential for (c) $[Au_{25}(SCH_2COOH)_{17}]^-$ and (d) $[Au_{25}(SCH_2CH_3)_{17}]^-$.

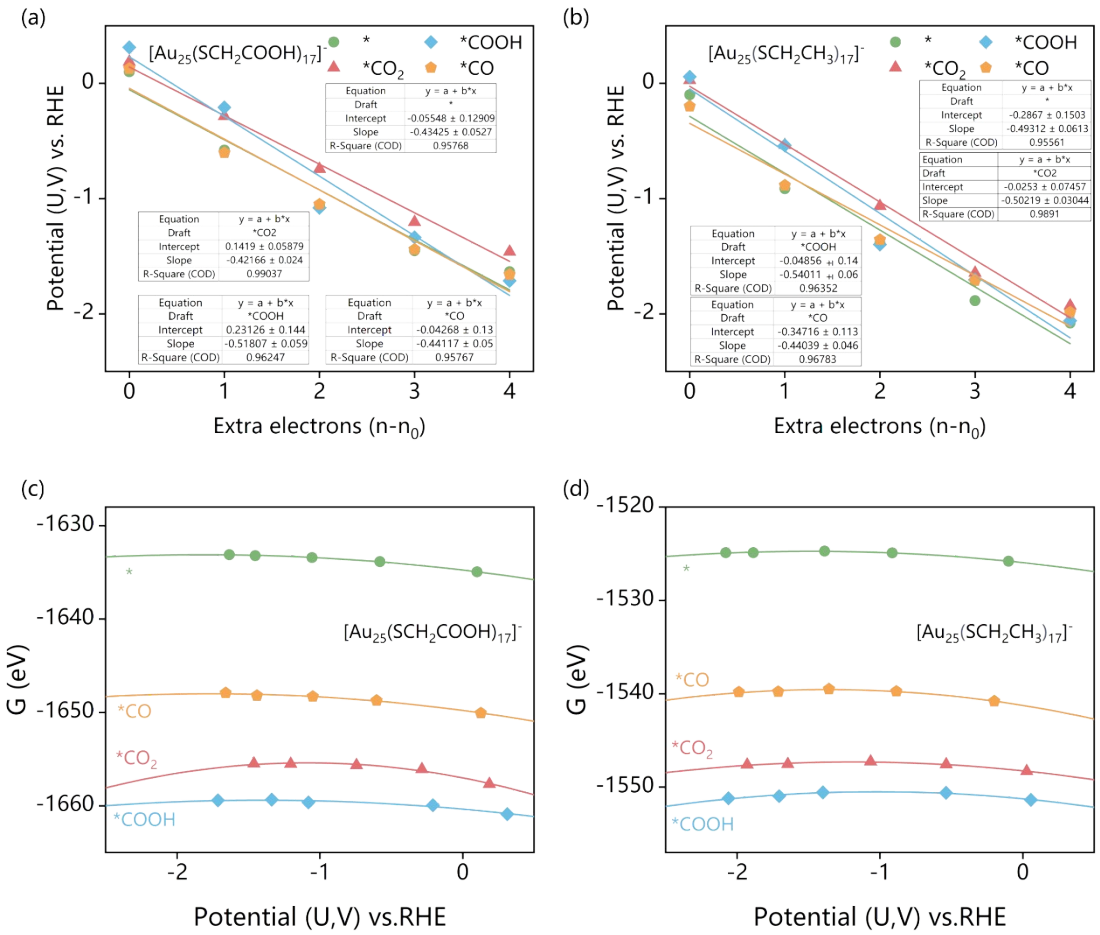

Fig. S6 The relationship between the number of extra electrons ($n–n_0$) and the corresponding electrode potentials for (a) $[Au_{25}(SCH_2COOH)_{17}]^-$ and (b) $[Au_{25}(SCH_2CH_3)_{17}]^-$ during the CO_2RR process. Variation in Gibbs free energy as a function of electrode potential for (c) $[Au_{25}(SCH_2COOH)_{17}]^-$ and (d) $[Au_{25}(SCH_2CH_3)_{17}]^-$.

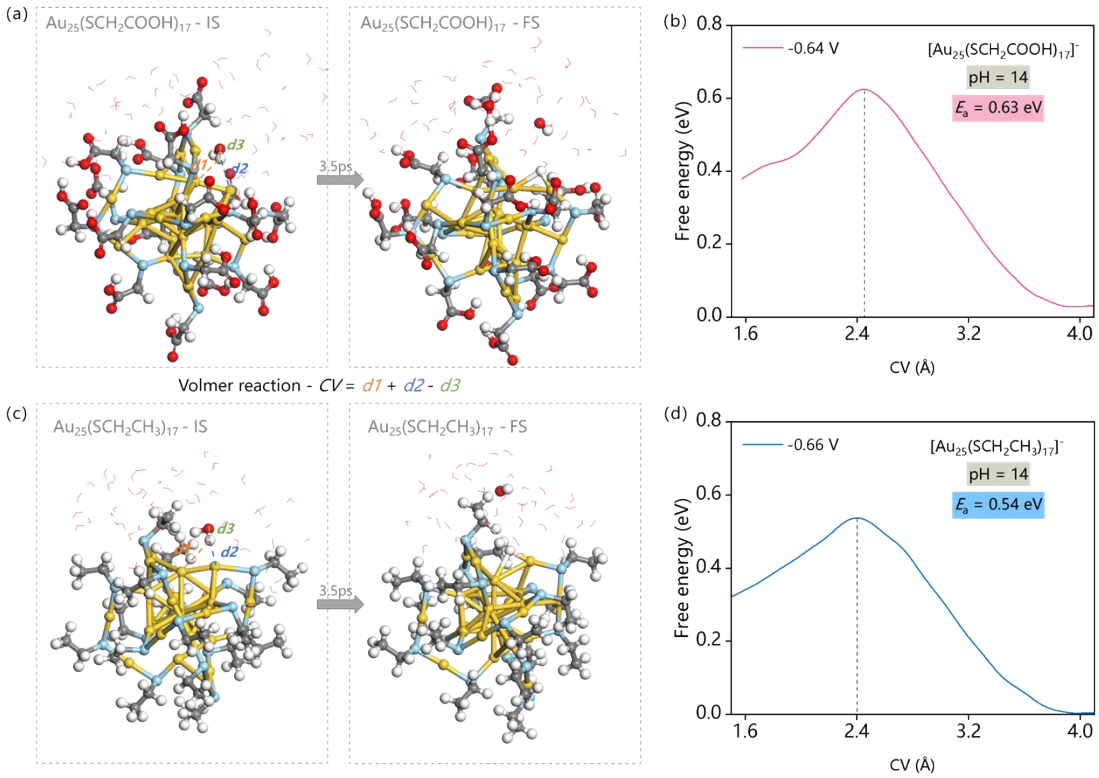

Fig. S7 Representative structures and energy profiles for the Volmer step in $[Au_{25}(SCH_2COOH)_{17}]^-$ and $[Au_{25}(SCH_2CH_3)_{17}]^-$ under similar potentials (vs RHE). (a, c) Initial state (IS) and final state (FS) structures for $[Au_{25}(SCH_2COOH)_{17}]^-$ and $[Au_{25}(SCH_2CH_3)_{17}]^-$, respectively. (b, d) Corresponding energy barriers sampled via SG-AIMD simulations for $[Au_{25}(SCH_2COOH)_{17}]^-$ and $[Au_{25}(SCH_2CH_3)_{17}]^-$.

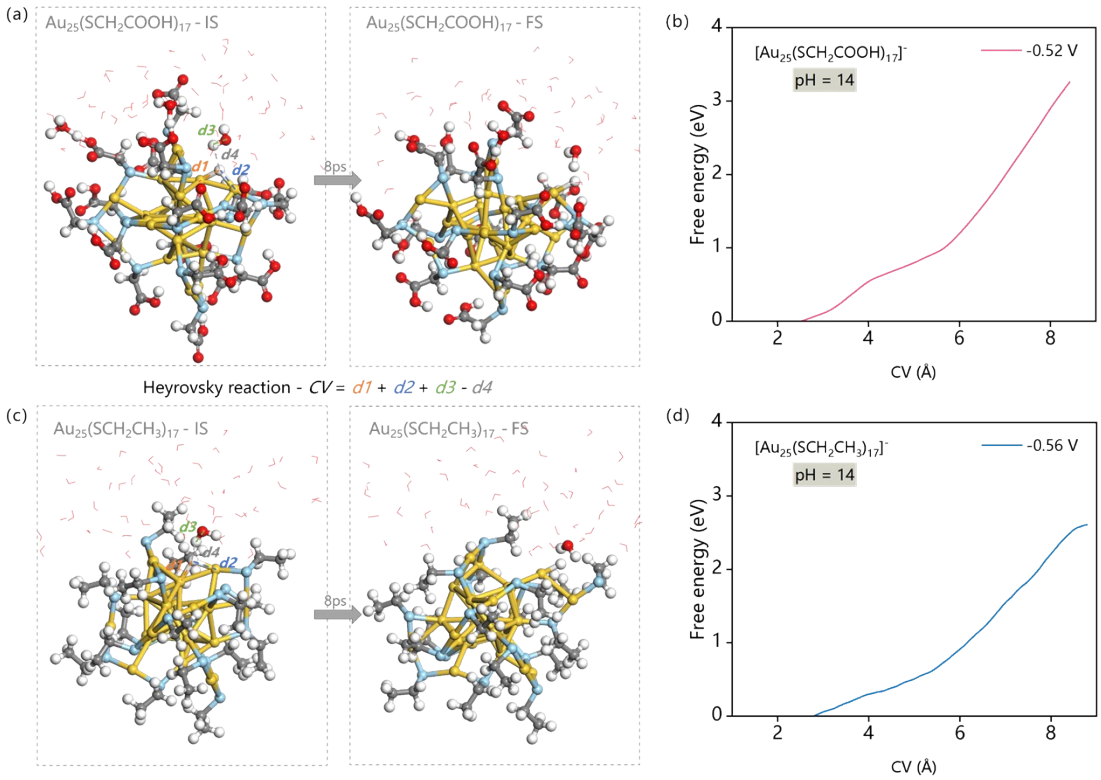

Fig. S8 Representative structures and energy profiles for the Heyrovsky step in $[Au_{25}(SCH_2COOH)_{17}]^-$ and $[Au_{25}(SCH_2CH_3)_{17}]^-$ under similar potentials (vs RHE). (a, c) Initial state (IS) and final state (FS) structures for $[Au_{25}(SCH_2COOH)_{17}]^-$ and $[Au_{25}(SCH_2CH_3)_{17}]^-$, respectively. (b, d) Corresponding energy barriers sampled via SG-AIMD simulations for $[Au_{25}(SCH_2COOH)_{17}]^-$ and $[Au_{25}(SCH_2CH_3)_{17}]^-$.

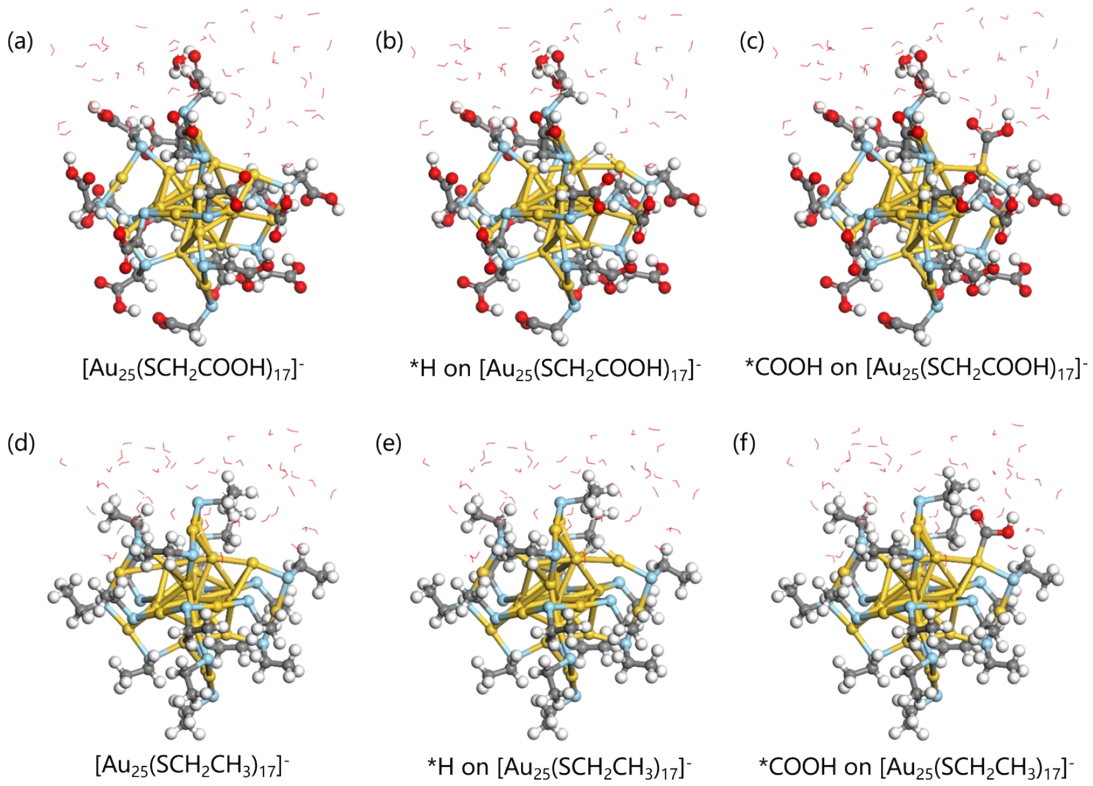

Fig. S9 Optimized structures of $[Au_{25}(SCH_2COOH)_{17}]^-$ and $[Au_{25}(SCH_2CH_3)_{17}]^-$ with key intermediates: (a) $[Au_{25}(SCH_2COOH)_{17}]^-$, (b) *H on $[Au_{25}(SCH_2COOH)_{17}]^-$, (c) *COOH on $[Au_{25}(SCH_2COOH)_{17}]^-$, (d) $[Au_{25}(SCH_2CH_3)_{17}]^-$, (e) *H on $[Au_{25}(SCH_2CH_3)_{17}]^-$, and (f) *COOH on $[Au_{25}(SCH_2CH_3)_{17}]^-$.

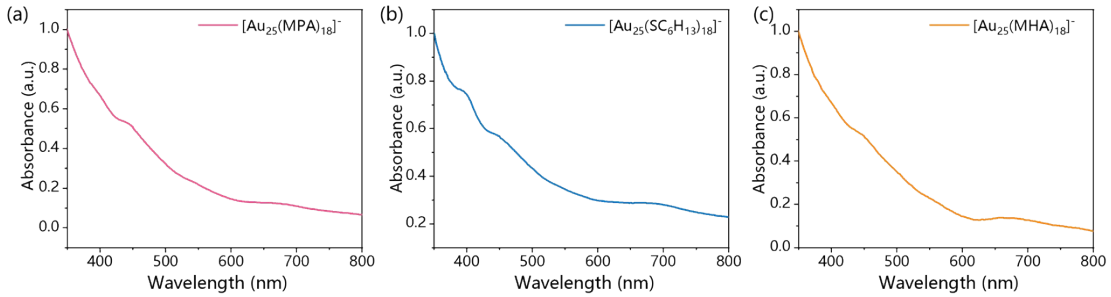

Fig. S10 The measured UV-vis absorption spectra of the synthesized (a) $[Au_{25}(MPA)_{18}]^-$, (b) $[Au_{25}(SC_6H_{13})_{18}]^-$, and (c) $[Au_{25}(MHA)_{18}]^-$ NCs.

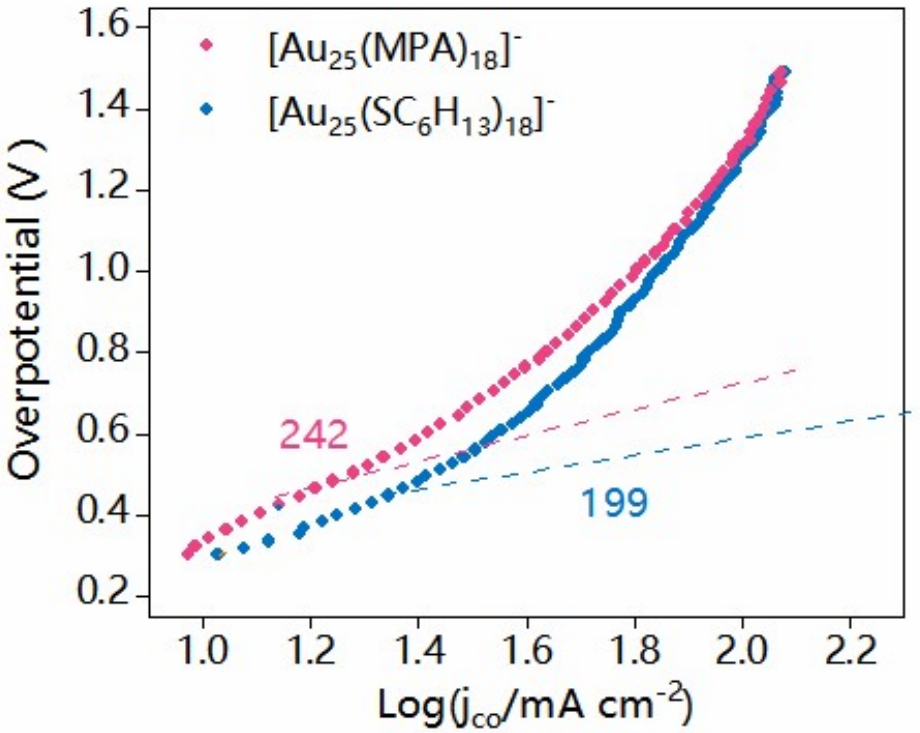

Fig. S11 Tafel slopes of the two Au_{25} catalysts in 1 M KOH solution saturated with CO_2.

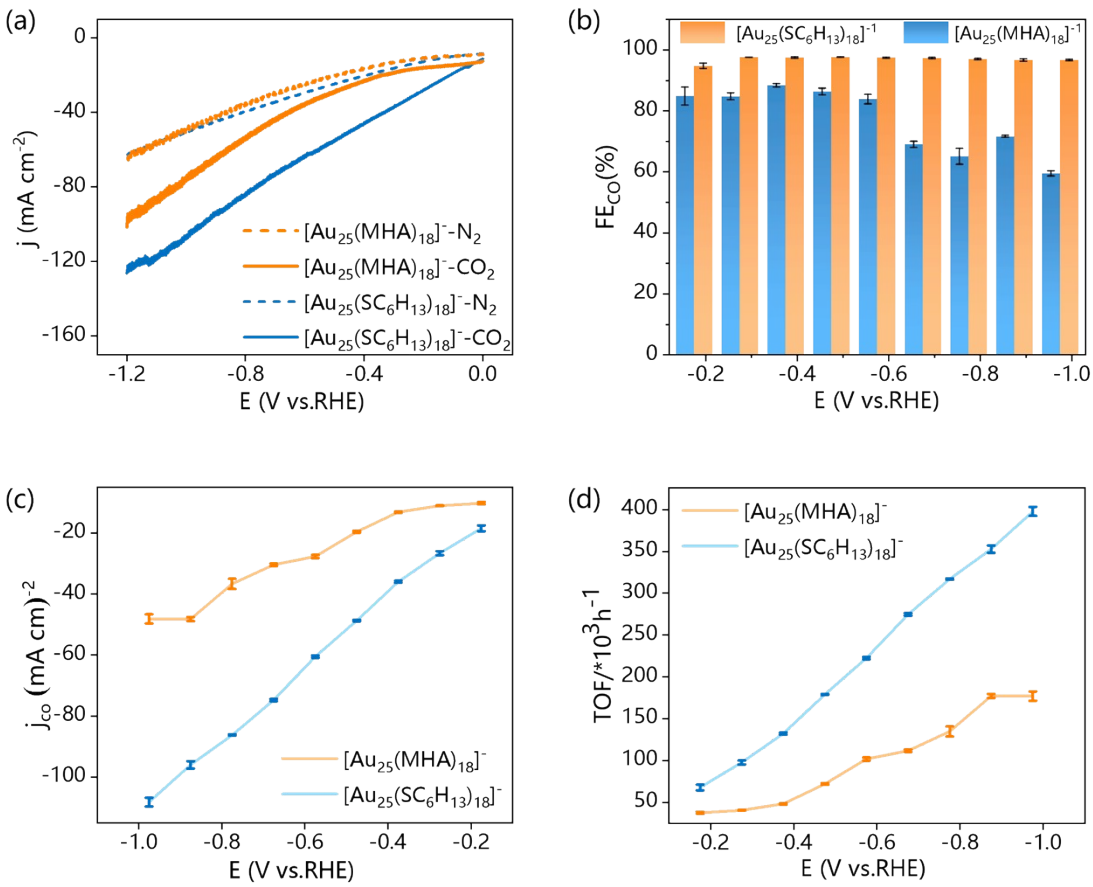

Fig. S12 Electrocatalytic CO_2RR performance in a CO_2 flow cell with 1M KOH electrolyte. (a) LSV curves of $[Au_{25}(MHA)_{18}]^-$ and $[Au_{25}(SC_6H_{13})_{18}]^-$ in N_2 and CO_2 environments. (b) FE_{CO} of $[Au_{25}(MHA)_{18}]^-$ and $[Au_{25}(SC_6H_{13})_{18}]^-$ at different potentials. (c) Fractional current density of CO at various potentials. (d) Turnover frequency (TOF) of CO at different potentials.

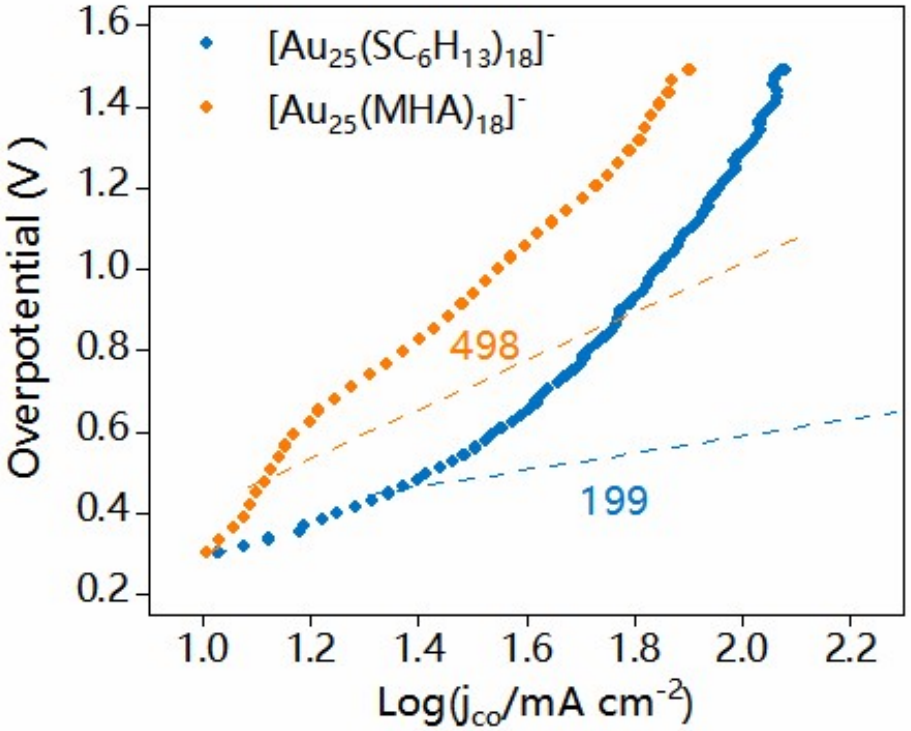

Fig. S13 Tafel slopes of $[Au_{25}(MHA)_{18}]^-$ and $[Au_{25}(SC_6H_{13})_{18}]^-$.

References

1. K. Mathew, V. Kolluru, S. Mula, S. N. Steinmann and R. G. Hennig, Implicit self-consistent electrolyte model in plane-wave density-functional theory, *J. Chem. Phys.*, 2019, **151**, 234101.
2. H. Zhao, H. Cao, Z. Zhang and Y.-G. Wang, Modeling the potential-dependent kinetics of CO_2 electroreduction on single-nickel atom catalysts with explicit solvation, *ACS Catal.*, 2022, **12**, 11380-11390.
3. H. Cao, Z. Zhang, J.-W. Chen and Y.-G. Wang, Potential-dependent free energy relationship in interpreting the electrochemical performance of CO_2 reduction on single atom catalysts, *ACS Catal.*, 2022, **12**, 6606-6617.
4. E. A. Carter, G. Ciccotti, J. T. Hynes and R. Kapral, Constrained reaction coordinate dynamics for the simulation of rare events, *Chem. Phys. Lett.*, 1989, **156**, 472-477.
5. M. Sprik and G. Ciccotti, Free energy from constrained molecular dynamics, *J. Chem. Phys.*, 1998, **109**, 7737-7744.